N-electron valence state perturbation theory based on density matrix renormalization group reference functions, with applications to chromium dimer and photovoltaic polymers

Sheng Guo, Mark A. Watson, Weifeng Hu, Qiming Sun, Garnet Kin-Lic Chan[1]
Department of Chemistry, Princeton University, Princeton, New Jersey 08544, USA

(Dated: 28 October 2015)

The second order n-electron valence state perturbation theory (NEVPT2) is a relatively cheap way to deal dynamic correlation without intruder state problem or level shift, while density matrix renormalization group (DMRG) is able to deal static correlation with a large active space and to provide reference wave functions needed in multireference perturbation theories. We present a method to combine DMRG and NEVPT2 (DMRG-NEVPT2) through the a general algorithm to compute high order reduced density matrices for DMRG wave function. The capacity of DMRG-NEVPT is demonstrated for calcualtions of chromium dimer potential energy curve and excited states energy of poly(p-phenylene vinylene).

I. INTRODUCTION

The density matrix renormalization group (DMRG)[1,2] has made it accessible to employ large active spaces for electronic structure problems in quantum chemistry. Nowadays, it has become quite straightforward to use DMRG as a robust numerical solver for static electron correlation problems. Examples are benchmark solutions of small molecules[3], transition metal clusters[4,5], also molecular crystals[6].

In chemical systems, electron interaction across large energy scales brings many other important chemistry, such as low-lying excited states in conjugated polymers, high-spin ground state in transition metals complexes. Qualitative and quantitative characterizations of these systems generally require correlating many electrons within a large number of orbitals. Direct treatment of such problem is generally impossible, but indirect methodology can apply, for example, by expanding the electron correlation outside active spaces. So far, there are methods which follow with this strategy with using large active spaces, for example, to apply perturbation theory to a large active space, or perform canonical transformation to get an effective Hamiltonian. The DMRG method has been embedded with the second-order perturbation theory[7,8], complete active space perturbation theory (CASPT), and canonical transformation(CT)[9], etc., to be extended for dynamic correlation. In these methods, high order reduced density matrices are generally needed, which are theoretically straightforward yet computationally non-trivial to compute.

In this work, we developed a general way to compute high order reduced density matrix (RDM) for DRMG wave functions. On the top of RDM calculations, we implemented the second order n-electron valence state perturbation theory (NEVPT2)[10–12], an intruder-state-free multireference perturbation theory, with DMRG reference wavefunctions, called DMRG-NEVPT2. Then we applied it to study potential energy curve of chromium dimer and excitation energies of the quasi-one dimensional photovoltaic molecule poly(p-phenylene vinylene) (PPV). The calculations for the potential energy curve of chromium dimer is one of the most notorious and demanding problem in ab-inito quantum chemistry. This system has been widely studied by many methods[7,13–19]. It is good system to demonstrate the capacity of DMRG-NEVPT2. PPV has always been of great interest by photophysists and photochemists, as it is well known for its charge-transfer properties upon photoexcitations[20,21]. The first optically bright state 1^1B_u whose polaronic feature is suggested to be responsible for the charge-transfer behavior, is estimated to lie below the 2^1A_g with a small gap of 0.7eV[22]. Many theoretical studies of PPV are based on model Hamiltonian, such as Pariser–Parr–Pople (PPP) model,[23,24] or semi-empirical quantum chemistry method[25]. However, ab initio quantum chemistry calculation were hardly reported due to the unaffordable computations to including the dynamic correlation and static correlation at the same time for such a system with many π orbitals, which need to be considered as active space in complete active space (CAS) calculations. With DMRG-NEVPT2, now it is possible to compute the excitation energies and energy orders of different states accurately.

II. THEORIES

A. DMRG wavefunction and optimization algorithm

As with other approximate wavefunction methods in quantum chemistry, DMRG is based on an approximate wvefunction ansatz. It is the matrix product state(MPS). A MPS is a non-linear wavefunction, built from contraction of tensors for each orbital in the basis. Limited by the dimension of tensors, called bond dimension, M, MPS could only explore a small subspace of Hilbert space. By increasing M, the MPS ansatz will give full configuration interaction (FCI) results. DMRG is a combination of renormalization and truncation algorithms to find a variational and optimal MPS. In practice, two

types of MPS are often used in DMRG calculations: an one-site and a two-site MPS.

The one-site MPS is defined as

$$|\Psi\rangle = \sum_{n_1,n_2\cdots n_p\cdots n_k} \mathbf{A}^{n_1}\mathbf{A}^{n_2}\cdots\mathbf{A}^{n_p}\cdots\mathbf{A}^{n_k} \quad (1)$$

Here, n_i is the occupacy of orbital i, one of $\{|\rangle, |\uparrow\rangle, |\downarrow\rangle, |\uparrow\downarrow\rangle\}$ and k is the number of orbitals. For a given n_i, $\mathbf{A}^{n_i}$ is $M \times M$ matrix, except that the first and last ones. For $\mathbf{A}^{n_1}$ and $\mathbf{A}^{n_k}$, their dimensions are $1 \times M$ and $M \times 1$ respectively. This ensures that for a given string $n_1 n_2 \cdots n_k$, a slater determinent, the $\mathbf{A}^{n_1}\mathbf{A}^{n_2}\cdots\mathbf{A}^{n_k}$ yields a scalar, the coefficient of the determinent $|n_1 n_2 \cdots n_k\rangle$

Similarly, the two-site MPS is defined as

$$|\Psi\rangle = \sum_{n_1,n_2\cdots n_p\cdots n_k} \mathbf{A}^{n_1}\mathbf{A}^{n_2}\cdots\mathbf{A}^{n_p,n_{p+1}}\cdots\mathbf{A}^{n_k} \quad (2)$$

In DMRG sweep algorithm, $\langle\Psi|\hat{H}|\Psi\rangle$ is variational optimized. And only a single tensor (A^{n_i} or $A^{n_i,n_{i+1}}$ for a two-site MPS) in the MPS is updated during the sweep at site i. It can be considered as solving eigenvalue problem of an effective Hamiltonian, which is a $4M^2 \times 4M^2$ matrix. This effective Hamiltonian is usually defined through complimentary operators ^{acitation}. The cost scaling is $O(k^2M^3)$ for this eighenvalue problem for one tensor and is $O(k^3M^3)$ for a whole sweep optimization.

Compared to an one-site MPS, a two-site MPS has more variational freedom and is able to change quantum numbers during the sweep. It helps avoid local minimum. However, the two-site MPS has N-representation problem: the converged two-site MPS is still different at different position of sweep. Based on a two-site MPS, expectation values, for example reduced density matrix, which often used to characterize a state and is essential for dynamic correlation calculations, have no unique results. Therefore, the strategy, "two-site to one-site" (a two-site MPS optimization followed by an one-site one), is widely used.

B. Reduced density matrix (RDM)

High order RDM is used for varied of post-CASSCF methods, such as multireference configuration interaction[?] and multireference perturbation theory[12,26], to include dynamic correlatons. For example, multireference perturbation theories, like CASPT2[26] and NEVPT2[12] (The details are in next subsection.), need up to fourth order RDM. Because in DMRG the orbital spaces are partitioned into several blocks, efficient RDM evaluation is not straight forward. The algorithms to build 2-RDm were proposed by several groups.[27,28] However, they are not feasible for higher order RDM, due to numerous "cases" of partition and types of operators. Here we introduce a general algorithm to generate a loop for every "case" and to skip redundant computations automatically.

From now on, when we refer a MPS, it means an one-site MPS, because it is needed in evaluation of RDM.

The 2-RDM is defined in this way

$$\gamma_{i,j,k,l} = \sum_{\sigma,\tau} \langle\Psi| a^\dagger_{i,\sigma} a^\dagger_{j,\tau} a_{k,\tau} a_{l,\sigma} |\Psi\rangle \quad (3)$$

It is similar for the higher order reduced density matrix.

It is not affordable to build and store k^{2N} operators used in N-RDM. And for RDM, the expectation value rather than the operators needed. There is no need to build these complicate operators. One efficient way is to distribute the indices (orbital label) i, j, k, l among different orbital subspace for diferent blocks in DMRG.[27,29] The complicate operators are the tensor product of small operators on different blocks. If small operators are contracted with the wave function before doing tensor product. The tensor product will become dot product of operators. It is much cheaper. Below are the details.

Operators like $\hat{a}^\dagger_i \hat{a}^\dagger_j \ldots \hat{a}_m \hat{a}_n \ldots$ can be permuted into a form like $\hat{o}_{i'}\hat{o}_{j'}\ldots\hat{o}_{m'}\hat{o}_{n'}$, with $i' \le j' \le \cdots \le m' \le n'$ and $\hat{o}$ is $\hat{a}$ or $\hat{a}^\dagger$. A string with N $\hat{a}$ and N $\hat{a}^\dagger$ determines the type of the operator. We call it "type pattern". Then the string is split into several small pieces according to blocks (orbital subgroups) in DMRG sweep.

There are three blocks in DMRG sweep algrithom. The system block ($\mathcal{S}$) is expanded during the sweep and the operators on it can be easy build on the flying. The dot block ($\mathcal{D}$) is composed of a single site and its operators are extremely simple and cheap. The environment block ($\mathcal{E}$) was computed from $\mathcal{S}$ in previous sweep in reverse direction, and its operators needed to be precomputed and stored (usually on disk). The $2N$ orbital labels of $\hat{O}$ is needed to be partitioned onto the three blocks. It is computational favorable to put more orbital labels on $\mathcal{D}$ and put few orbital labels on $\mathcal{E}$. And the numbers of orbital labels on $\mathcal{S}$ and $\mathcal{E}$ need to be balanced, otherwise number of operators on one block will be extremely big. For most RDM element (not for element like $\gamma_{0,0,0,0}$), at least one orbital label could be put on $\mathcal{D}$ and at most $N-1$ orbital labels on $\mathcal{E}$ by change the position of the dot site. The set $\{n_\mathcal{S}, n_\mathcal{D}, n_\mathcal{E}\}$ determines the numbers of orbital labels on different blocks. It is called "number pattern". In general, every number pattern is valid if the number of orbital labels on $\mathcal{S}$ is no more than N, that on $\mathcal{D}$ is no more than 4 and that on $\mathcal{E}$ is no more than $N-1$, except the edge cases for the first step and last step in the sweep (in the appendix). And nearly every "type pattern" could be combined with all "number patterns" if with some restrictions (in appendix).

With above process, the types of operators needed on $\mathcal{S}$, $\mathcal{D}$, and $\mathcal{E}$ are determined for each pattern ("type pattern" and "number pattern"). Loop the orbital labels

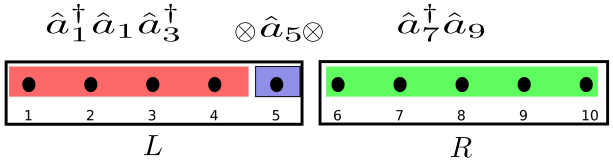

FIG. 1. Evaluation of a three RDM element $\gamma_{1,3,7;1,5,9}$. $\hat{a}_1^\dagger \hat{a}_1 \hat{a}_3^\dagger$ is on $\mathcal{S}$, $\hat{a}_5$ is on $\mathcal{D}$, and $\hat{a}_7^\dagger \hat{a}_9^\dagger$ is on $\mathcal{E}$. It belongs to (3,1,2) "number pattern" and $(\hat{a}^\dagger \hat{a} \hat{a}^\dagger \hat{a} \hat{a}^\dagger \hat{a})$ "type pattern".

of operators, we can build all operators we need. There are about $O(N^k)$ operators, most of which are on $\mathcal{S}$. The computation for generate these operators are $O(k^N M^3)$ for one step at the sweep and are $O(k^{N+1} M^3)$ in total.

After building operators on each block, $\hat{O}^S$, $\hat{O}^D$, $\hat{O}^E$, combine $\hat{O}^S$ and $\hat{O}^D$ into O^L, a big left block $\mathcal{S} \otimes \mathcal{D}$. (Combining $\mathcal{E}$ and $\mathcal{D}$ only for RDM calcualtions is also feasible.) The $\mathcal{E}$ is the right block. RDM element $\gamma = \sum_{l,r} \sum_{l',r'} c_{l,r} O^L_{l,l'} O^R_{r,r'} c_{l',r'}$, with $|\Psi\rangle = c_{l,r} |l\rangle |r\rangle$, can be computed in two step. (1) $X_{r,r'} = \sum_l \sum_{l'} c_{l,r} O^{l,l'} c_{l',r'}$. (2) $\gamma = \sum_{r,r'} X_{r,r'} O^R_{r,r'}$. The reason for contracting wave function with O^L first is that the dimension of O^L is $4M$ while the dimension of O^R is M. The number of operation required for forming X is $O(k^{N+1} M^3)$ and that for dot product between X and O^R is $O(k^{2N} M^2)$. The computations for N-RDM are $O(k^{N+1} M^3 + k^{2N} M^2)$.

With above process, an expectation value like $\langle \hat{a}_0^\dagger \hat{a}_1^\dagger \hat{a}_2 \hat{a}_3 \rangle$ is obtained. For a non-spinadapted DMRG algrithm (the operators in not a spin tensor), we can get the value of $\gamma_{0,1,3,2}$ by permuting $\hat{a}_2$ and $\hat{a}_3$. For spinadapted DMRG operators, what we get is a set of $\langle \hat{a}_0^\dagger \hat{a}_1^\dagger \hat{a}_2 \hat{a}_3 \rangle$ values. They are $\langle \{[(\hat{a}_0^\dagger \hat{a}_1^\dagger)^{S_1}_{\mathcal{S}} (\hat{a}_2)_{\mathcal{D}}]^{S_2} (\hat{a}_3)_{\mathcal{E}} \}^{S_3} \rangle$ with different spins S_1, S_2, S_3. The spin tensors can be expanded as linear combination of spin orbital operators and linear equations are formed for spin orbital RDM elements. With spin embeding, expectation values of all spin tensors with non-zero spin are zero, significantly decrease the number of expectation values to compute. The coefficiencies for these linear equations are the same for the operators in the same pattern and can be generated autmaticaly and be reused. Computation cost for this process is not related the bond dimension, M and is ignorable compared to other parts.

The computation of 4RDM, which is needed in DMRG-NEVPT is $O(k^8 M^2 + k^5 M^3)$, much higher than that of DMRG optimization. Therefore, the bond dimension of MPS in 4RDM calculations is limited. With the same bond dimension, MPS from a "reverse schedule" sweep is usually better optimized that MPS from standard sweep schedule, in which the bond dimension is increased. All of our NEVPT calculations use MPS optmized through "reverse schedule".

C. N-electron valance state perturbation theory

In this section, we briefly review the strongly contracted NEVPT2[11,12], a second-order multireference perturbation theory. The target zero-order wave function is defined as

$$P_{CAS} H P_{CAS} |\Psi^{(0)}_m\rangle = E^{(0)}_m |\Psi^{(0)}_m\rangle \tag{4}$$

with $P_{CAS} = \sum_{I \in S} |I\rangle \langle I|$ is the projector onto the CAS space.

The zero order Hamiltonian is chosen in the form give by Dyall[30]:

$$H^D = H_i + H_v + C \tag{5}$$

where H_i is a one-electron (diagonal) operator in non-active subspace:

$$H_i = \sum_{i,\sigma}^{core} \epsilon_i \hat{a}^\dagger_{i,\sigma} \hat{a}_{i,\sigma} + \sum_{r,\sigma}^{virt} \epsilon_r \hat{a}^\dagger_{r,\sigma} \hat{a}_{r,\sigma} \tag{6}$$

where ϵ_i and ϵ_r are orbital energies.

H_v is a two-electron operator confined to the active space:

$$H_v = \sum_{ab,\sigma}^{act} h^{eff}_{ab} \hat{a}^\dagger_{a,\sigma} \hat{a}_{b,\sigma} + \sum_{abcd,\sigma_1,\eta}^{act} \langle ab|cd\rangle \, \hat{a}^\dagger_{a,\sigma} \hat{a}^\dagger_{b,\eta} \hat{a}_{d,\eta} \hat{a}_{c,\sigma} \tag{7}$$

where $h^{eff}_{ab} = h_{ab} + \sum_i^{core} (2 \langle ai|bi\rangle - \langle ai|ib\rangle)$

and C is a constant to ensure that H^D is equivalent to the full Hamiltonian within the CAS space.

The zero order wave functions external to the CAS space, referred to as the "perturbers", belong to CAS-CI spaces with well defined patterns of the inactive (core+virtual) orbitals and with a given number of active electrons. The perturber functions are written as $|\Psi^{(k)}_{l,\mu}\rangle$ and the corresponding CAS-CI spaces as $S^{(k)}_l$, where k is the number of electrons promoted to $(k > 0)$ or removed from $(k < 0)$ the active space, l denotes the pattern of inactive orbitals and μ numerates the various perturbers.

In stongly contracted NEVPT2, utilizes just one function from each $S^{(k)}_l$ subspace, $|\Psi^{(k)}_l\rangle = S^{(k)}_l H |\Psi^{(0)}_m\rangle$ with energy given by

$$E^{(k)}_l = \frac{\langle \Psi^{(k)}_l | H^D |\Psi^{(k)}_l\rangle}{\langle \Psi^{(k)}_l | \Psi^{(k)}_l\rangle} \tag{8}$$

And the zero order Hamiltonian becomes

$$H_0 = |\Psi^{(k)'}_l\rangle E^{(k)}_l \langle \Psi^{(k)'}_l| + |\Psi^{(0)}_m\rangle E^{(0)}_m \langle \Psi^{(0)}_m| \tag{9}$$

where $|\Psi^{(k)'}_l\rangle$ is normalized $|\Psi^{(k)}_l\rangle$

The bottle neck is the evaluation of energies of perturbers, where up to forth order RDM is needed. 4-RDM is contracted with double electron integral in active space to form auxiliary matrices.[12] In our implementation for DMRG-NEVPT2, 4-RDM is computed on the fly, avoiding storing huge 4-RDM.

Like Kurashige and Yanai's implementation of DMRG-CASPT2[7], these auxiliary matrices can be computed with a scaling similar with that of 3-RDM by make special types of operators, which are the contraction of integral and creation (and annihilation) operators. However, the two-electron Hamiltonian in NEVPT2 is much more complex that the Fork operators (which is diagonal if canonical orbitals used) in CASPT2. Many types of contracted operators would be needed in DMRG frame. It is the very hard to implement and the prefactor is big, even though the scaling is better. Therefore, We only contracted integral and operators in CASCI-NEVPT2, not in DMRG-NEVPT2.

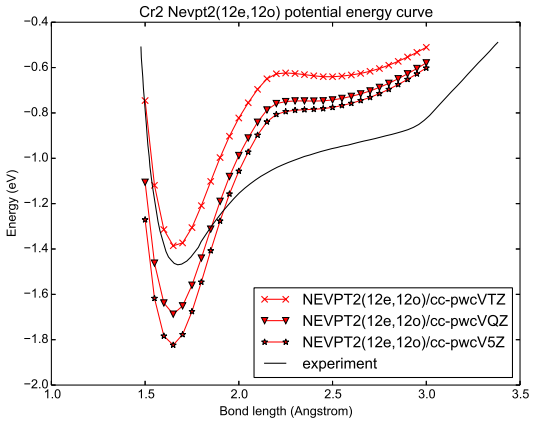

FIG. 2. NEVPT2(12e,12o) potential energy curve with a suite cc-pwcVXZ (X=T,Q,5) basis set

III. APPLICATIONS

A. Chromium dimer

Chromium dimmer has been a challenging problem in quantum chemistry, because large active space is needed to simulate its potential energy curve correct. At the same time, dynamic correlation is also required for a qualitative potential energy curve.[7,13,15,16,19,31–33]

The CAS(12e,12o), derived from the 3d and 4s atomic orbitals, was widely employed for chrmium dimer calculations.[15,16,19,31–33] Both CASPT2[31–33] and NEVPT2[11] based CASSCF(12e,12o) reference function overestimate the dissociation energy of the 3d-3d bond, especially when large basis sets, e.g. g-, h-, or even i- type function, were used.[14,15] And the results from CASPT2(12e,12o) are heavily sensitive to the choice of the zero-order Hamiltonian.[14,17] According to NEVPT3 study,[15] the common CAS(12e,12o) wave function is not a good starting reference for the perturbation theory, because the third-order perturbation results in an large fluctuation and an unreasonably curve. DMRG-CASPT2 calculation with a CAS(12e,28o), derived from 3d, 4s, 4p, 4d atomic orbitals, gave potential energy curves close to the experimental one. However, different zero-order Hamiltonians, due to different level shifts in CASPT2, gave quantitatively different results. The difference of D_e with different level shifts was about 0.2eV.[7] DMRG-NEVPT2 is free of intruder state and there is no need add "level shift" to change zero-order Hamiltonian. It should be feasible to discribe chromium dimer potential energy curve.

A suite of cc-pwcVXZ (X = T,Q,5) basis sets was used in our calculations. No basis set superposition error (BSSE) corrections were applied in the calculations because the BSSE was regarded as small for the large basis sets including h or i-type functions. The X2C Hamiltonian was used to include scalar relativistic effects. The DMRG and corresponding RDM calculations were performed with Block[34]. All the other calculations were done in Pyscf[35]. The energy of isolated atoms was set as zero.

For the NEVPT2(12e,12o) potential energy curve of Cr_2 in III A, larger basis set gives a deeper and worse curve. It agreed with previous studies with atomic natural orbital (ANO) basis sets.[15] Then the CAS(12e,12o) was extended by adding another set of σ, π, π', δ, δ' orbitals and their corresponding anti bond orbitals from external orbitals, forming a CAS(12e,22o). DMRG are neccesary here to avoid exponentially increasing computations of FCI. These additional active orbitals were chosen based on the symmetry and orbital energies; thus their dominant compoents were are from $4p$ and $4d$ orbitals at first. After DMRG-CASSCF orbital optimization ($M = 1000$ and there is no frozen core), only $4d$ orbitals component remained. Actually, a 3d double-shell was included in active space, which is reported to greatly increase results of transition metal[36]. After DMRG-CASSCF orbital optimization, the reference MPS was optimized with $M = 4000$. Then the MPS was compressed into a MPS with $M = 800$ through "reverse schedule", before doing DMRG-NEVPT2 calcualations. To check whether $M = 800$ is big enough, the DMRG-NEVPT2 energies with cc-pwcV5Z basis for geometry points near minimum were also calculated with $M = 1200$. The difference between curving with $M = 800$ and that with $M = 1200$ is very small. Finally, the (TZ/QZ/5Z) results were extrapolated to the complete basis set (CBS) limit in exponential formula for DMRG-CASSCF energy and in l^{-3} formula for DMRG-NEVPT2 correction energy.

Figure III A shows the potential energy curve with a suite of cc-pwcVXZ (X=T,Q,5) basis set and the complete basis set (CBS) limit. A larger basis set gives a deeper and better curve. The CBS limit potential en-

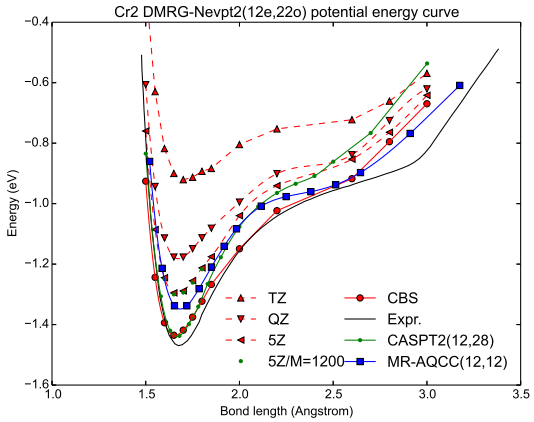

FIG. 3. DMRG-NEVPT2(12e,22o)(M=800) potential energy curve with a suite of cc-pwcVXZ (X=T,Q,5) basis set and the complete basis set (CBS) limit. The experimental curve is taken from Ref. 37DMRG-CASCPT2(12e,28o) curve is from Ref. 7 and the MR-AQCC(12e,12o) is from Ref. 16.

TABLE I. Spectroscopic Constants for the ground state of Cr_2 from different methods

	$D_e(eV)$	R_0(Å)	ω_e
DMRG-NEVPT2(12e,22o)	1.436	1.656	476
DMRG-CASPT2(12e,28o)[a]	1.61	1.681	480
MR-AQCC(12e,12o)[b]	1.355	1.685	459
experiment[c]	1.47(5)	1.679	480.6(5)

[a] DMRG-CASPT2(12e,28o)/$g_1(M=\infty)$ in Ref. 7
[b] Ref. 16
[c] Ref. 37

ergy curve agreed with the experimental well, with the exception of the strong bend at about 2.8Å, where the reliability of the RKR potential in this region has alreadybeen questioned before.[13]

DMRG-NEVPT2(12e,22o) results were nearly the same with DMRG-CASPT2(12e,28o)[7] results for the $3d$ bond region. However, for the $4s$ bond ("shoulder") region, the DMRG-NEVPT2(12e,22o) results were closer to the exerimental one, even though their CAS did not include $4p$ orbitals while DMRG-CASPT2 did. It is reasobalbe. Because, in the $4s$ bond region, the correlation is strong, because the d orbitals are not well bonded and nearly degenerate. The Fock operator, monoelectron zero order Hamiltonian in CASPT2, is not good enough. The comparision between DMRG-NEVPT2(12e,22o) and DMRG-CASPT2(12e,28o) also indicates, together with the fact that only $4d$ orbitals remained in the active space after orbital optimization, $4d$ orbitals are more important than $4p$ orbitals for the static correlation and the reference function.

B. Poly(p-phenylene vinylene)

Poly(p-phenylene vinylene) is a type of phenyl-based light emitting conjugated polymers, which is useful for displays and photovoltaic devices. It has many low-lying states that participate in the photophysics and it was extensively investigated through theoretical methods, sush as DMRG based on Pariser–Parr–Pople (PPP) model[23,24] and semi-empirical intermediate neglect of differential overlap (INDO) Hamiltonian with configuration interaction[25]. However, ab initio correlated wave function calculations were not often reported, because of the difficulty to include static and dynamic correlation together for a complex system. We used PPV-3 as an example and demonstrated how to predict the excitation energies for low-lying state through DMRG-NEVPT2 calculation and the accuracy of DMRG-NEVPT2 for conjugated polymer molecule.

The cc-pVDZ basis was chosen for the calcualtions and an active space was chosen from 22 conjugated π orbitals. For the ground state S_0, we obtained the initial equilibrium geometry of PPV-3 via DMRG-CI geometry optimization with an interface between Block and orca[38], starting from a guess from DFT/B3LYP optimized geometry. The geometry optimization was first run at M = 1000, and then near the convergence at M = 2000. Canonical orbitals are used in the geometry optimization.

Then state-averaged calculations were performed for ^1A_g (2 states) and B_u symmetry (3 states), with canonical orbitals of the ground state. To identify excited states, we computed the transition 1-RDM and transition 2-RDM from the ground state, and identified the state according to a dominant excitation signature. Based on the chosen active space, 3^1B_u is identified as the first optically bright state, with a HOMO→ LUMO excitation signature. And 2^2A_g in state-average calculation with 2 staets (3^2A_g when more states were averaged) is the first dark state, with a HOMO-1→ LUMO + HOMO→ LUMO+1 and HOMO,HOMO→ LUMO,LUMO excitation signature. Due to lack of dynamic correlation ($\sigma-\pi$ interaction), the energy order of excited states is significantly different with experimental results or calculations with PPP model.

After including dynamic correlation through DMRG-NEVPT2, the energy first bright state was much lowered and it became the first excited state (1^1B_u). This is similar to low-lying excited states of polyenes, where dynamic correlations lower the ionic excited state (1^1B_u) relative to covalent excited state (2^1A_g) However, the energy order did not converge with the bond dimension in the calculation (Table II).

Localized orbitals usually give a better convergence for DMRG calculation.[5] Therefore, further DMRG-NEVPT2 calculations were carried out based on split-localized orbitals (localize the occupied and unoccupied π orbitals separately with Pipek-Mezey method[39]). The NEVPT2 energies were calculated for lowest 6 states

TABLE II. Excitation energy (eV) calculated from DMRG-NEVPT2 with canonical orbitals. States are labeled according to energies with M= 750.

state	M=250	M=500	M=750	DMRG-CI(M=750)
2^1A_g	4.742	4.669	4.657	4.991
1^1B_u	4.027	4.191	4.180	5.269
2^1B_u	4.449	4.486	4.264	4.740
3^1B_u	5.090	4.328	4.600	5.132

TABLE III. Excitation energy (eV) calculated from DMRG-NEVPT2 with localized orbitals. States are labeled according to excitation signatures and energies with M= 750.

state	M=500	M=750	DMRG-CI(M=750)
1^1B_u	3.8628	3.8625	5.1312
2^1B_u	4.4980	4.4978	4.4953
2^1A_g	4.6634	4.6634	4.8456
3^1B_u	4.8268	4.8262	4.7542
4^1B_u	4.8441	4.8443	4.7572

(based on DMRG-CI energy). The excitation energies were converged into less than $0.6meV$with bond dimension (Table III). They were accurate enough to determine the energy order of low-lying excite states. The difference between calculated excitation energies from canonical orbital and those from local orbitals was big, and it might not be the same even when bond dimension is infinite. One reason is that the molecular geometry was optimized without symmetry restriction. Some integral terms, which should be zero according symmetry, were not exact zero. When local orbital orbitals were used, the symmetry restriction on the integral was removed.

The excitation energy of first bright state (3.86eV) agrees well with results from other theoretical studies (3.88eV[25], 3.91eV[23]). However, it deviated from the experimental value (3.5eV[40],3.43eV[41]) a lot. The reasons were that PPV oligomer was substituted with tertiary butyl end-group to become soluble in the experiment and that the solvent was not considered in the calculations.

IV. CONCLUSION

In this work, we developed a general algorithm to compute different order RDMs for DMRG wave function, which can be used by many dynamic correlation methods. Through up to 4th order RDM, we combined DMRG and NEVPT2, a intruder state free second order multireference perturbation theory, to discribe static and dynamic correlations at the same time, forming DMRG-NEVPT2 method. It made the calculations complex molecules with large active spaces possible.

To demonstrate the capability of DMRG-NEVPT2 method, we used this method to calculate the potential energy curve of chromium dimer and excited states of poly(p-phenylene vinylene). For chromium dimer, the extended active space included $4d$ orbitals and the so called "double d" effect were considered. It gave quantatively corrected potential energy curves, demonstrating that correlation from second shell orbitals were essential for chromium dimer. For light emitting conjugated polymers, Poly(p-phenylene vinylene), excitation energy of low-lying excited states were computed through DMRG-NEVPT2 with different orbitals in active space. The local orbitals calculation gave results converged with bond dimension much better than canonical orbitals. And the accuracy from local orbital DMRG-NEVPT2 is about $0.6meV$, relative to standard NEVPT2. While the environments were not included in the calculations, the energy order of excited states were reasonable.

Based on above two examples, DMRG-NEVPT2 is a intruder free perturbation methods and it can be used for the molecule where large active spaces are needed.

ACKNOWLEDGEMENTS

APPPENDIX A: EDGE CASES FOR NUMBER PATTERNS IN RDM

All number patterns in N-RDM, $\{n_{\mathcal{S}},n_{\mathcal{D}},n_{\mathcal{E}}\}$, need to be computed if

$$0 \leq n_{\mathcal{S}} \leq N \tag{10}$$
$$0 \leq n_{\mathcal{E}} \leq N-1 \tag{11}$$
$$1 \leq n_{\mathcal{D}} \leq 4 \tag{12}$$
$$n_{\mathcal{S}} + n_{\mathcal{D}} + n_{\mathcal{E}} = 2N \tag{13}$$
$$\tag{14}$$

However, for some RDM elements, whose indices cannot be aranged as what we discribed above, because too many their indices lie in first or last site. We need additional number patterns to compute them.

For the first step of DMRG sweep, additional patterns are added. These patterns satisfies

$$N+1 \leq n_{\mathcal{S}} \leq min(4,2N) \tag{15}$$
$$0 \leq n_{\mathcal{D}} \leq 4 \tag{16}$$
$$n_{\mathcal{S}} + n_{\mathcal{D}} + n_{\mathcal{E}} = 2N \tag{17}$$
$$\tag{18}$$

For the last step of DMRG sweep, additional patterns are also added. These patterns satisfies

$$N \leq n_{\mathcal{E}} \leq min(4,2N) \tag{19}$$
$$0 \leq n_{\mathcal{D}} \leq 4 \tag{20}$$
$$n_{\mathcal{S}} + n_{\mathcal{D}} + n_{\mathcal{E}} = 2N \tag{21}$$
$$\tag{22}$$

Because $\mathcal{S}$ (or $\mathcal{E}$) is composed of single site, expectation value of an operator with more than two $\hat{a}$ or two $\hat{a}^\dagger$ on it is zero. The number of indices on single sites should not be more than 4.

APPPENDIX B: RESTRICTION ON TYPE PATTERNS IN RDM

It is a waste of resource to compute RDM element which is zero or redundant. And the RDM element can be computed through multiple types of combinations of operators in different blocks. We implemented some restrictions to skip calculations for zero and redundant RDM elements.

The operators $\hat{a}_i$ and $\hat{a}_j^\dagger$ are permutated to make their orbitals indices not decrease. Only the permutation between two operators with different orbital indices are needed. If $\hat{a}_i$ is ahead of $\hat{a}_j^\dagger$ and $i = j$, the compound operators are not needed in RDM calcualtion. For a single site block, the type with $\hat{a}$ ahead of $\hat{a}^\dagger$ is omitted. For other blocks, the loop of for $\hat{o}_i\hat{o}_j\hat{o}_k\dots$ should be $i \le j \le k\dots$ ($=$ is only valid when the two nearby operators in normal order).

And the RDM (not transition RDM) is symmetry matrix. Use 3-RDM as example

$$\langle \hat{a}_i^\dagger \hat{a}_j^\dagger \hat{a}_k^\dagger \hat{a}_l \hat{a}_m \hat{a}_n \rangle = \langle (\hat{a}_i^\dagger \hat{a}_j^\dagger \hat{a}_k^\dagger \hat{a}_l \hat{a}_m \hat{a}_n)^\dagger \rangle = \langle \hat{a}_n^\dagger \hat{a}_m^\dagger \hat{a}_l^\dagger \hat{a}_k \hat{a}_j \hat{a}_i \rangle \tag{23}$$

We can always use transpose and permutation to make operators begin with $\hat{a}^\dagger$ rather than $\hat{a}$ (the beginning is the operator with smallest orbital indice). Therefore, all types pattern begin with $\hat{a}$ is omitted.

Similarly, if operators begin with $\hat{a}_i^\dagger \hat{a}_i$, $\hat{a}_i^\dagger \hat{a}_i \hat{a}_j^\dagger \hat{a}_j$ or $\hat{a}_i^\dagger \hat{a}_i \hat{a}_j^\dagger \hat{a}_j \hat{a}_k^\dagger \hat{a}_k$, the remaining part of operators also has transpose and permutation symmetry.

$$\begin{aligned} &\langle \hat{a}_i^\dagger \hat{a}_i (\hat{o}_j \hat{o}_k \dots) \rangle \\ =&\langle ((\hat{a}_i^\dagger \hat{a}_i (\hat{o}_j \hat{o}_k \dots))^\dagger \rangle \\ =&\langle (\hat{o}_j \hat{o}_k \dots)^\dagger (\hat{a}_i^\dagger \hat{a}_i)^\dagger \rangle \\ =&\langle \hat{a}_i^\dagger \hat{a}_i (\hat{o}_j \hat{o}_k \dots)^\dagger \rangle \end{aligned} \tag{24}$$

where $i < j \le k \dots$

Therefore, there is no need to compute the types operators in which $\hat{a}$ follows $\hat{a}_i^\dagger \hat{a}_i$.

[1] S. R. White, Physical Review Letters **69**, 2863 (1992).
[2] S. R. White, Physical Review B **48**, 10345 (1993).
[3] G. K.-L. Chan and M. Head-Gordon, The Journal of Chemical Physics **116**, 4462 (2002).
[4] S. Sharma, K. Sivalingam, F. Neese, and G. K.-L. Chan, Nature Chemistry **6**, 927 (2014).
[5] R. Olivares-Amaya, W. Hu, N. Nakatani, S. Sharma, J. Yang, and G. K.-L. Chan, The Journal of Chemical Physics **142**, 034102 (2015).
[6] J. Yang, W. Hu, D. Usvyat, D. Matthews, M. Schtz, and G. K.-L. Chan, Science **345**, 640 (2014).
[7] Y. Kurashige and T. Yanai, The Journal of Chemical Physics **135**, 094104 (2011).
[8] S. Sharma and G. K.-L. Chan, The Journal of Chemical Physics **141**, 111101 (2014).
[9] E. Neuscamman, T. Yanai, and G. K.-L. Chan, International Reviews in Physical Chemistry **29**, 231 (2010).
[10] C. Angeli, R. Cimiraglia, S. Evangelisti, T. Leininger, and J.-P. Malrieu, The Journal of Chemical Physics **114**, 10252 (2001).
[11] C. Angeli, R. Cimiraglia, and J.-P. Malrieu, Chemical Physics Letters **350**, 297 (2001).
[12] C. Angeli, R. Cimiraglia, and J.-P. Malrieu, The Journal of Chemical Physics **117**, 9138 (2002).
[13] B. O. Roos, Collection of Czechoslovak Chemical Communications **68**, 265 (2003).
[14] P. Celani, H. Stoll, H.-J. Werner, and P. J. K. *, Molecular Physics **102**, 2369 (2004).
[15] C. Angeli, B. Bories, A. Cavallini, and R. Cimiraglia, The Journal of Chemical Physics **124**, 054108 (2006).
[16] T. Mller, The Journal of Physical Chemistry A **113**, 12729 (2009).
[17] F. Ruiprez, F. Aquilante, J. M. Ugalde, and I. Infante, Journal of Chemical Theory and Computation **7**, 1640 (2011).
[18] Y. Kurashige, Molecular Physics **112**, 1485 (2014).
[19] S. Sharma and A. Alavi, The Journal of Chemical Physics **143**, 102815 (2015).
[20] J. H. Burroughes, D. D. C. Bradley, A. R. Brown, R. N. Marks, K. Mackay, R. H. Friend, P. L. Burns, and A. B. Holmes, Nature **347**, 539 (1990).
[21] R. H. Friend, R. W. Gymer, A. B. Holmes, J. H. Burroughes, R. N. Marks, C. Taliani, D. D. C. Bradley, D. A. D. Santos, J. L. Brdas, M. Lgdlund, and W. R. Salaneck, Nature **397**, 121 (1999).
[22] S. J. Martin, D. D. C. Bradley, P. A. Lane, H. Mellor, and P. L. Burn, Physical Review B **59**, 15133 (1999).
[23] A. Shukla, Physical Review B **65**, 125204 (2002).
[24] R. J. Bursill and W. Barford, The Journal of Chemical Physics **130**, 234302 (2009).
[25] D. Beljonne, Z. Shuai, R. H. Friend, and J. L. Brdas, The Journal of Chemical Physics **102**, 2042 (1995).
[26] K. Andersson, P. A. Malmqvist, B. O. Roos, A. J. Sadlej, and K. Wolinski, The Journal of Physical Chemistry **94**, 5483 (1990).
[27] D. Ghosh, J. Hachmann, T. Yanai, and G. K.-L. Chan, The Journal of Chemical Physics **128**, 144117 (2008).
[28] D. Zgid and M. Nooijen, The Journal of Chemical Physics **128**, 144115 (2008).
[29] D. Zgid and M. Nooijen, The Journal of Chemical Physics **128**, 144116 (2008).
[30] K. G. Dyall, The Journal of Chemical Physics **102**, 4909 (1995).
[31] K. Andersson, B. O. Roos, P. . Malmqvist, and P. O. Widmark, Chemical Physics Letters **230**, 391 (1994).
[32] B. O. Roos and K. Andersson, Chemical Physics Letters **245**, 215 (1995).
[33] B. O. Roos, K. Andersson, M. P. Flscher, P.-. Malmqvist, L. Serrano-Andrs, K. Pierloot, and M. Merchn, in *Advances in Chemical Physics*, edited by I. Prigogine and S. A. Rice (John Wiley & Sons, Inc., 1996) pp. 219–331.
[34] S. Sharma and G. K.-L. Chan, The Journal of Chemical Physics **136**, 124121 (2012).
[35] "https://github.com/sunqm/pyscf,".
[36] K. Andersson and B. O. Roos, Chemical Physics Letters **191**, 507 (1992).
[37] S. M. Casey and D. G. Leopold, The Journal of Physical Chemistry **97**, 816 (1993).
[38] F. Neese, Wiley Interdisciplinary Reviews: Computational Molecular Science **2**, 73 (2012).
[39] J. Pipek and P. G. Mezey, The Journal of Chemical Physics **90**, 4916 (1989).
[40] H. S. Woo, O. Lhost, S. C. Graham, D. D. C. Bradley, R. H. Friend, C. Quattrocchi, J. L. Brdas, R. Schenk, and K. Mllen, Synthetic Metals **59**, 13 (1993).
[41] G. H. Gelinck, J. J. Piet, B. R. Wegewijs, K. Mllen, J. Wildeman, G. Hadziioannou, and J. M. Warman, Physical Review B **62**, 1489 (2000).